J. Phys. B: At. Mol. Opt. Phys. **31** (1998) 911–924. Printed in the UK PII: S0953-4075(98)88189-3

Time-independent and time-dependent close-coupling methods for the electron-impact ionization of Mg^+, Al^{2+} and Si^{3+}

N R Badnell†, M S Pindzola‡, I Bray§ and D C Griffin‖

† Department of Physics and Applied Physics, University of Strathclyde, Glasgow G4 0NG, UK
‡ Department of Physics, Auburn University, Auburn, AL 36849, USA
§ Electronic Structure of Materials Centre, The Flinders University of South Australia, GPO Box 2100, Adelaide 5001, Australia
‖ Department of Physics, Rollins College, Winter Park, FL 32789, USA

Received 6 October 1997

Abstract. The electron-impact ionization cross sections of Mg^+, Al^{2+} and Si^{3+} are calculated using both time-independent and time-dependent close-coupling methods. The time-independent methods are *R*-matrix and convergent close-coupling solutions based on a total wavefunction constructed using antisymmetrized products of Laguerre pseudo-orbitals and physical bound orbitals. The time-dependent method is based on the propagation of wavepackets constructed using excited-state orbitals calculated in a core pseudo-potential. The results of all three methods are in good agreement for Mg^+; there is also good agreement between the *R*-matrix and time-dependent methods for Al^{2+} and Si^{3+}, and all three methods yield ionization cross sections that lie substantially above the experimental crossed-beams measurements of Crandall *et al*. There is better accord with the crossed-beams measurements of Peart *et al* for Mg^+, but the theoretical results still lie 10% higher at 50 eV. Some disagreement is noted, for both Al^{2+} and Si^{3+}, between the convergent close-coupling results and the *R*-matrix and time-dependent results.

1. Introduction

Recently, several *ab initio* theoretical methods have been developed which, for the first time, have the capability of producing accurate electron-impact ionization cross sections for atoms and their ions. Common to all of the methods is the coupling of the initial states (before ionization) to the final states (after ionization). The convergent close coupling (Bray and Stelbovics 1993), the hyperspherical close coupling (Kato and Watanabe 1995), the *R*-matrix with pseudo-states (Bartschat and Bray 1996a), and the time-dependent close-coupling (Pindzola and Schultz 1996, Pindzola and Robicheaux 1996) methods have all produced ionization cross sections for hydrogen in excellent agreement with experiment. We note, however, some interesting differences between time-independent (Bartschat and Bray 1996b) and time-dependent (Pindzola and Robicheaux 1997) results for the differential cross sections (in ejected energy), which have been attributed to a lack of convergence in the pseudo-state expansion of the former—in fact an infinite expansion appears to be necessary (Bray 1997). However, this does not affect total ionization cross sections. The convergent close-coupling (Bray and Fursa 1995, 1996) and *R*-matrix with pseudo-states (Hudson *et al* 1996) methods have also produced accurate cross sections for the electron-impact ionization of helium. Since accurate electron-impact ionization cross sections for atomic

0953-4075/98/040911+14$19.50

ions are needed for the modelling of a variety of laboratory and astrophysical plasmas, it is important to extend the range of atomic systems that can be treated by these advanced methods.

When Bray (1995) extended the convergent close-coupling method to calculate electron-impact ionization cross sections for low-charged ions in the Li isoelectronic sequence, he found serious discrepancies between the results of theory and crossed-beams experiments on Be^+, B^{2+}, and C^{3+}. Recently, Bartschat and Bray (1997a) repeated the convergent close-coupling calculations for the ionization of Be^+ and carried out *R*-matrix calculations, using a small pseudo-state expansion, while Pindzola *et al* (1997) carried out time-dependent close-coupling and *R*-matrix calculations, using a large pseudo-state expansion, for the same ion as well. All of the results confirmed the serious discrepancy between theory and experiment for Be^+. Also, Marchalant *et al* (1997) carried out convergent close-coupling calculations and *R*-matrix calculations for the (excitation and) ionization of B^{2+} which appear to confirm the experimental underestimate for ionization, although the *R*-matrix results fell significantly below the convergent close-coupling results above 80 eV; this was attributed to the small pseudo-state expansion used in the *R*-matrix calculations.

In this work, we use time-independent and time-dependent close-coupling methods to calculate electron-impact ionization cross sections for the Na-like ions Mg^+, Al^{2+}, and Si^{3+}, for which crossed-beams measurements have been made by Crandall *et al* (1982). Before the onset of the contributions from excitation followed by autoionization, their results lie substantially below the distorted-wave Born-exchange results of Younger (1981), both for Mg^+ and Al^{2+}, but are broadly consistent with them for Si^{3+}. For the case of Mg^+, crossed-beams measurements using an energy-resolved electron beam have been made by Peart *et al* (1991) and their results lie significantly above the results of Crandall *et al* (1982). The time-dependent close-coupling method that we use is based on the propagation of wavepackets and their projection onto a complete set of bound excited states. As in the case of Be^+ (Pindzola *et al* 1997), to go beyond the previous work on the electron-impact ionization of hydrogen (Pindzola and Robicheaux 1996), we calculate the excited-state spectrum using a pseudo-potential for the core electrons. The pseudo-potential method has the added benefits of keeping the lattice size relatively small and eliminating problems with superelastic scattering. The time-independent methods are based on *R*-matrix and convergent close-coupling calculations using a large pseudo-state basis. In particular, our *R*-matrix approach is similar in spirit to that of the convergent close-coupling approach in that we aim for convergence in our cross section to a few per cent with our pseudo-state expansion, while retaining the power of the *R*-matrix method to generate results at many energies efficiently. This is in contrast to the *R*-matrix approach of Bartschat and Bray (1996a, b, 1997a, b) in which the average result of a number of *R*-matrix runs is taken, each made with a small pseudo-state expansion and a different radial scaling parameter. A further correction is then made to the ionization cross section to take account of the limited number of pseudo-states that they use to represent the continuum (typically one or two for the highest angular momentum).

The structure of this paper is as follows. The time-independent theories are reviewed in section 2.1, the time-dependent theory is reviewed in section 2.2, and the results of the three methods are compared with each other and with experiment in section 3. We close with a short conclusion.

2. Theory

2.1. Time-independent theories

2.1.1. R-matrix. We use an L^2-basis to represent the bound and continuum states of the ion (see, e.g., Yamani and Reinhardt 1975). Excitation of the positive energy states corresponds to ionization. A more accurate approach, especially at low energies, is to project the positive *and* negative energy L^2-states onto the true physical continuum. We use the program AUTOSTRUCTURE (Badnell 1986) to generate an orthogonal set of Laguerre basis orbitals (Badnell and Gorczyca 1997). We use physical orbitals for those states that we wish to study transitions between, or from. The N-electron configurations are built-up from the one-electron orbitals and then the Hamiltonian is diagonalized to obtain the set of N-electron eigenenergies and eigenstates. For both Mg^+ and Al^{2+}, we used three different bases to enable us to determine the convergence of our L^2 expansion. For all three bases we use physical orbitals for 1s through 4f (i.e. 10 in all). The 1s through 3s orbitals were determined initially from a single-configuration Hartree–Fock calculation using the package due to Froese Fischer (1991). The Ne-like core was then frozen and the remaining (valence) orbitals determined, again from a single-configuration calculation. These orbitals were then input to AUTOSTRUCTURE, the Laguerre orbitals generated, and the resulting term energies studied for their distribution about the ionization limit. Basis I used pseudo-orbitals ($\overline{nl}$) up to $\overline{n} = 12$ and for $\bar{l} = 0$–3, i.e. an additional eight pseudo-orbitals (and hence eight pseudo-states) per angular momentum. Basis II used basis I plus eight g-orbitals. Basis III used basis II plus an extra three s-orbitals, two p-orbitals and one d-orbital giving rise to a 53 term close-coupling expansion consisting of 13 s-states, 12 p-states, 11 d-states, 9 f-states and 8 g-states. Of these, 8, 7, 7, 6 and 6, respectively, lie above the ionization limit. A further refinement can be considered. If the initial positioning of the pseudo-state term energies is such that one (or more) lies close to the ionization limit then the $\lambda_{\overline{nl}}$ scaling parameters on the Laguerre orbitals (see equation (1) of Badnell and Gorczyca 1997) can be adjusted (and hence the term energies) to ensure that the ionization limit lies roughly midway between two term energies of the same symmetry, for each symmetry. This reduces the size of the effect of projection, which is an additional approximation. In the case of Mg^+ and Si^{3+}, the default scaling parameter values of unity gave rise to a reasonable distribution of term energies around the ionization limit. But for Al^{2+}, a better distribution was obtained on using the following values for the scaling parameters for the Laguerre orbitals: $\lambda_{\overline{ns}} = 1.07$, $\lambda_{\overline{np}} = 0.93$, $\lambda_{\overline{nd}} = 1.03$, $\lambda_{\overline{nf}} = 0.99$, and $\lambda_{\overline{ng}} = 0.875$. This was only done for basis III.

We solve the time-independent close-coupling equations using the R-matrix method (Burke and Berrington 1993). Our starting point is RMATRX I, the (Breit–Pauli) R-matrix codes (Berrington *et al* 1995) developed for the Iron Project (Hummer *et al* 1993). A practical problem encountered is the orthogonalization of the continuum basis orbitals (that are used to describe the scattering electron) to the Laguerre orbitals. Bartschat *et al* (1996) use a numerical Schmidt orthogonalization procedure. We use an alternative approach which we find to be more stable numerically when using a large R-matrix continuum basis (see Badnell and Gorczyca 1997, Gorczyca and Badnell 1997). For Mg^+ (Al^{2+}) [Si^{3+}], our 'target' orbitals necessitate the use of an R-matrix box of radius $R = 43.6$ ($R = 29.5$) [$R = 21.5$] and 30 (30) [22] continuum basis orbitals per angular momentum (initially) to obtain cross sections converged to 1% up to an incident electron energy of 55 eV (80 eV) [100 eV]. We carried out LS-coupling calculations with exchange, as described above, for $L = 0$–15 together with a small 'top-up' for higher L.

The 'top-up' merits further discussion. We use Seaton's STGF asymptotic code (see Berrington *et al* 1987). The original version used by the Opacity Project only topped-up dipole transitions in LS-coupling, which often suffices for the excitation of physical discrete states. (Versions in use by the Iron Project also top-up fine-structure transitions.) This is insufficient for the excitation of pseudo-states. For example, on using basis I at 50 eV for Mg^+ we find that 50% of the total ionization cross section comes from $3s \rightarrow \overline{nf}$ transitions. Furthermore, for the $L = 8$ partial wave $3s \rightarrow \overline{nf}$ transitions contribute 75% of the partial cross section. The reason for this bias towards high multipole transitions (in contrast to the normal 'physical' case) is that unitarity forces convergence of the total cross section (i.e. summed-over all $\bar{l}$) before convergence is achieved in the partial cross sections (i.e. each individual $\bar{l}$)—see Bray (1994b) for a detailed study. So, topping-up only the dipole and the quadrupole transitions, for example, gives rise to a severe underestimate of the high-L contribution. We top-up using the lowest positive 2^λ-pole for each transition. The top-up itself is based on the Burgess (1974) sum rule for dipole transitions and a series in $(k_</k_>)^{2L+1}$ and/or $L^{-2\lambda+1}$ for higher multipoles (see Burgess *et al* 1970). A by-product of this work is that it is now possible to include, independently, the lowest 2^λ-pole perturbing potential in the solution of the coupled equations for the outer region. This has its largest percentage effect (10%) on the (small) high-L partial cross sections.

In our work on Be^+ (Pindzola *et al* 1997) we determined the ionization cross section simply by summing-up the cross sections to the positive energy pseudo-states. A more refined treatment is warranted for Mg^+, and is applied to Al^{2+} and Si^{3+} as well. Following Gallaher (1974), we determine our ionization cross section from

$$\sigma_{\rm ion} = \sum_{\overline{n}} \left[1 - \sum_{n} |\langle n|\overline{n}\rangle|^2 \right] \sigma_{\overline{n}}, \tag{1}$$

where $|\overline{n}\rangle$ denotes a positive or negative energy pseudo eigenstate, $\sigma_{\overline{n}}$ is the excitation cross section (from the initial ground state) to $|\overline{n}\rangle$, and $\langle n|$ denotes a physical discrete eigenstate. The $|\overline{n}\rangle$ and $\langle n|$ are themselves configuration-mixed states of the original target basis resulting from diagonalization of the N-electron Hamiltonian. This 'target algebra' is already conveniently available from STG2 of the R-matrix code following our earlier work on the distorted-wave approximation (Gorczyca *et al* 1994). The sum over $\overline{n}$ is dominated by those pseudo-states that lie just above and below the ionization limit. The sum over n is over all physical discrete states and its evaluation requires the overlaps between the pseudo-orbitals and a Rydberg series of physical orbitals. These are available conveniently from AUTOSTRUCTURE which was originally developed to sweep efficiently through entire Rydberg series. The point about this (approximate) form of the projection is that it takes place on the cross sections, not the scattering matrix, and so can be applied as a simple post-processing exercise after STGF has been run. Our coding of the projection is quite general and is not restricted to quasi-one-electron systems.

2.1.2. Convergent close coupling. The convergent close-coupling theory for the targets under consideration has been given by Bray (1994a), and reviewed by Bray and Stelbovics (1995). It has been applied to the calculation of electron-impact total ionization cross sections of sodium (Bray 1994b), and lithium-like targets (Bray 1995). The method relies on treating the target continuum via a set of square-integrable pseudo-states obtained from diagonalization of the target Hamiltonian in an orthogonal truncated Laguerre basis. The size of the basis is increased until convergence, in the observable of interest, is attained to a desired accuracy. The Laguerre basis is chosen so that we can be sure that simply increasing the basis size improves 'completeness'.

In this sense, the convergent close-coupling approach is similar to the R-matrix with pseudo-states method described above. However, it lacks the strength of the R-matrix approach in that it calculates only a single energy at a time. On the other hand, it is as applicable at 1 eV as at 1 keV and is able to handle excitation to higher excited states which lie outside of a typical R-matrix box. The reason for the difference between the two approaches is that the (convergent) close-coupling equations are formed and solved in momentum space. This involves the solution of a set of linear equations, after the kernel matrix elements have been evaluated. The length of a convergent close-coupling calculation is dominated by the calculation of the kernel matrix elements (an N_r^2 process, where N_r is the rank of the matrix) and the solution of the linear equations (an N_r^3 process). The length of a large R-matrix calculation is also dominated by an N_r^3 process, namely diagonalization of the $(N+1)$-electron Hamiltonian.

In these calculations, we first carry out a single configuration Hartree–Fock calculation to determine the 1s, 2s, and 2p orbitals. These are used to generate a frozen-core potential for the Ne-like core to reduce the atom to a quasi-one-electron atom. Then, a large Laguerre orbital basis is diagonalized in the frozen-core potential and the resulting 1s, 2s and 2p orbitals are discarded. Specifically, we use a basis from which remain: 18 s-states, 18 p-states, 17 d-states, 15 f-states and 12 g-states. The exponential fall-off parameters λ for Mg^+, Al^{2+} and Si^{3+} are taken to be approximately 2, 3 and 4, respectively ($\lambda/2z$ is equivalent to the $\lambda_{\overline{nl}}$ used in section 2.1.1). In fact, we vary λ at each total energy E so as to ensure that the integration rule associated with the pseudo-states has E as one of the endpoints (Bray and Clare 1997). This minimizes the problem with pseudo-resonances and gives an estimate of the accuracy of the results by observing any deviation from expected smooth cross sections. The projection technique is applied (see equation (1)), but its effect is found to be relatively small.

2.1.3. Distorted wave. We use a non-exchange distorted-wave approximation based on a triple partial wave expansion of the first-order perturbation theory scattering amplitude, both to provide the contribution from higher partial waves ($L > 6$) for a hybrid calculation with the time-dependent method and as a check on the time-independent close-coupling results at high-L—these are sensitive to the largest target angular momentum state included in the pseudo-state expansion. The incident and scattered electrons are calculated in a V^N distorting potential, while the bound and ejected electrons are calculated in a V^{N-1} potential (Younger 1980). In previous work on the electron-impact ionization of hydrogen (Pindzola and Robicheaux 1996), this choice of potentials for the distorted-wave method was found to give fairly good cross sections at high angular momentum. We find that the non-exchange distorted-wave *partial* cross sections converge to the close-coupling ones much more rapidly than those obtained from calculations that include exchange do. We note that our distorted-wave with exchange *total* cross sections are smaller and more accurate than our non-exchange distorted-wave *total* cross sections (as are those of Younger's (1981)) as the latter method grossly overestimates the *low-L* partial cross sections.

2.2. Time-dependent theory

The time-dependent close-coupling theory for electron scattering from atomic ions involving one electron outside of a closed shell has been given by Pindzola *et al* (1997). Since the method is a wavepacket solution of the time-dependent Schrödinger equation, the need for three-body Coulomb asymptotic forms is avoided. The coupled partial differential equations for each LS symmetry are solved on a two-dimensional lattice using an explicit

time propagator. The numerical algorithm is easily implemented on massively parallel supercomputer platforms such as the Cray T3E-600 and Intel Paragon machines used in this study. The initial LS radial wavefunction is constructed as an antisymmetrized product of an incoming radial wavepacket for the scattering electron and a bound orbital for the valence electron. Following the collision, the electron-impact excitation and ionization cross sections are calculated by projecting the time-evolved radial wavefunction onto a complete set of single-particle states for the valence electron.

The closed-shell orbitals are obtained by solving their corresponding Hartree–Fock equations (Froese Fischer 1991). The core orbitals are then used to construct the radial Hamiltonian:

$$h(r) = -\frac{1}{2}\frac{\partial^2}{\partial r^2} + V^{\ell}_{HX}(r), \tag{2}$$

where

$$V^{\ell}_{HX}(r) = \frac{\ell(\ell+1)}{2r^2} - \frac{Z}{r} + V_H(r) - \frac{\alpha_\ell}{2}\left(\frac{24\rho}{\pi}\right)^{\frac{1}{3}}, \tag{3}$$

$V_H(r)$ is the Hartree potential, and ρ is the probability density. The excited-state spectrum is obtained by diagonalizing $h(r)$ on the lattice. The parameter α_ℓ is varied to obtain experimental energy splittings for the first few excited states.

If we choose the model potential, V^{ℓ}_{HX}, for use in the time-dependent close-coupled equations then we run into problems associated with superelastic scattering (Pindzola *et al* 1997). To solve this problem, we introduce pseudo-potentials into the time-dependent method. Using standard procedures (Christiansen *et al* 1979), we first generate a lowest-energy pseudo-orbital for each angular momentum occupied in the core. Essentially, all of the inner nodes of the previously generated lowest-energy valence orbital are removed in a smooth manner. An ℓ-dependent pseudo-potential (V^{ℓ}_{PP}) is obtained by inverting the radial Schrödinger equation with the newly constructed pseudo-orbital. The new radial Hamiltonian:

$$h(r) = -\frac{1}{2}\frac{\partial^2}{\partial r^2} + V^{\ell}_{PP}(r), \tag{4}$$

is then diagonalized on the lattice to obtain an excited pseudo-state spectrum. For Na-like ions, the ns and np radial orbital spectra are replaced by $\overline{n\mathrm{s}}$ and $\overline{n\mathrm{p}}$ radial pseudo-orbital spectra. This eliminates the unphysical superelastic scattering.

The time-dependent close-coupling equations were solved for electron scattering from Mg^+ at incident energies of 30, 40 and 50 eV, from Al^{2+} at 45, 60, and 80 eV, and from Si^{3+} at 70, 80 and 90 eV. We employed a 250×250 lattice for Mg^+ with each radial direction from $0 \rightarrow 50$ and a 200×200 lattice for both Al^{2+} and Si^{3+} with each radial direction from $0 \rightarrow 40$. In all cases the lattice was spanned by a uniform mesh with spacing $\Delta r = 0.2$. Between 3000 and 15 000 time steps were needed to propagate each of the 14 LS symmetric wavepackets before cross section convergence was achieved. The number of coupled partial differential equations ranged from 4 for the ^{1}S wavepacket to 16 for the ^{3}I wavepacket. The computer resources required by the time-dependent method are comparable with those required by the time-independent methods.

3. Results

None of the theoretical calculations allow for excitations out of the Ne-like core. Consequently, we focus our results and interest on energies that lie below the first excitation–autoionization threshold. This lies at ≈ 50 eV for Mg^+, ≈ 75 eV for Al^{2+} and ≈ 100 eV

Table 1. Partial ionization cross sections (10^{-18} cm^2) at an incident energy of 30 eV for Mg^+.

^{2S+1}L	Distorted-wave (non-exchange)	Time-dependent close-coupling	*R*-matrix close-coupling	Convergent close-coupling
^{1}0	0.318	0.353	0.402	0.460
^{3}0	0.954	0.072	0.072	0.138
^{1}1	1.487	1.263	1.707	2.299
^{3}1	4.463	0.577	0.888	0.947
^{1}2	3.016	3.561	4.352	4.394
^{3}2	9.050	2.164	2.975	2.901
^{1}3	3.353	7.981	8.809	8.842
^{3}3	10.058	1.660	2.137	2.103
^{1}4	2.049	5.459	5.407	5.630
^{3}4	6.149	1.868	2.216	2.245
^{1}5	1.444	4.060	4.020	4.295
^{3}5	4.333	2.570	2.663	2.926
^{1}6	1.344	3.308	3.174	3.114
^{3}6	4.033	2.113	1.931	2.192

for Si^{3+}. All of the *R*-matrix results presented here were obtained using basis III unless stated otherwise. In the figures, the *R*-matrix cross sections for Mg^+ (Al^{2+} and Si^{3+}) have been convoluted with a 2 eV (4 eV) FWHM Gaussian function so as to average over small pseudo-resonance features.

3.1. Mg^+

Partial ionization cross sections for Mg^+ at 30 eV and 50 eV are presented in tables 1 and 2 where we compare the close-coupling results with themselves and with distorted-wave results. At 30 eV, we note that the time-dependent ^{3}P, ^{3}D, and ^{3}F results lie 20–30% below the time-independent results, which are in much closer agreement with each other. By 50 eV, we see that the *R*-matrix and convergent close-coupling partial cross sections differ by no more than 5%, except for ^{1}P, ^{1}F, and ^{1}G, where the difference is still less than 10%. The time-dependent results again differ somewhat more from the time-independent results—typically by 20% for ^{3}P, ^{3}D and ^{3}F, while by $L = 6$ the difference is less than 10%. The distorted-wave results for the singlet and triplet partials are in the ratio of 1:3 of course. From the time-independent close-coupling results, we see that exchange effects start to fall-off from $L = 8$ and achieve a 1:2.6 ratio at $L = 12$ and a 1:3.0 ratio at $L = 15$. The (small) difference between the distorted-wave and time-independent results at high-L is due possibly to the omission of H-states in the latter calculations; this is by analogy with the comparison of our *R*-matrix results for bases I and II. We find that the addition of G-states affects the high partial waves only and so only starts to affect the total cross section at high energy. Although exchange is not negligible at $L = 7$, we see that there is close accord between distorted-wave and close-coupling for the sum of the singlet and triplet partial cross sections for a given L, i.e. there is a tendency for exchange effects to cancel here. (As noted in section 2.1.3, allowance for exchange within the distorted-wave approximation itself actually gives worse results.) Thus, it is possible to use these distorted-wave results to supplement the $L = 0$–6 time-dependent results to enable us to obtain total ionization cross sections, in a hybrid form. (Indeed, in general, distorted-wave partial cross sections could and should be used to 'top-up' the time-independent close-coupling partial cross sections as well since they can be evaluated much more efficiently.) These hybrid results are compared

Table 2. Partial ionization cross sections (10^{-18} cm^2) at an incident energy of 50 eV for Mg^+.

^{2S+1}L	Distorted-wave (non-exchange)	Time-dependent close-coupling	*R*-matrix close-coupling	Convergent close-coupling
^{1}0	0.305	0.255	0.255	0.266
^{3}0	0.915	0.170	0.163	0.153
^{1}1	1.029	1.089	1.141	1.248
^{3}1	3.087	0.784	0.991	1.012
^{1}2	1.918	2.128	2.111	2.224
^{3}2	5.753	2.171	2.795	2.771
^{1}3	2.423	5.148	5.050	5.453
^{3}3	7.269	2.334	2.787	2.936
^{1}4	1.763	4.294	4.252	3.872
^{3}4	5.290	2.004	2.346	2.244
^{1}5	1.575	3.828	3.842	3.626
^{3}5	4.726	2.280	2.401	2.466
^{1}6	1.321	3.453	3.227	3.124
^{3}6	3.964	2.030	2.002	2.123
^{1}7	1.110		2.464	2.380
^{3}7	3.330		1.835	1.937
^{1}8	0.888		1.697	1.695
^{3}8	2.663		1.727	1.715
^{1}9	0.656		1.077	1.066
^{3}9	1.967		1.445	1.439
^{1}10	0.449		0.594	0.578
^{3}10	1.347		1.056	1.053
^{1}11	0.290		0.321	0.312
^{3}11	0.869		0.718	0.716
^{1}12	0.179		0.175	0.169
^{3}12	0.538		0.458	0.447
^{1}13	0.108		0.099	0.094
^{3}13	0.323		0.279	0.269
^{1}14	0.064		0.057	0.054
^{3}14	0.191		0.168	0.160
^{1}15	0.037		0.034	0.032
^{3}15	0.112		0.101	0.096

Table 3. Total ionization cross sections (10^{-18} cm^2) for Mg^+.

Energy (eV)	Time-dependent + distorted-wave	*R*-matrix close-coupling	Convergent close-coupling
30	46.4	48.2	49.2
40	49.2	49.2	50.1
50	47.3	48.0	47.9

with the results of the time-independent close-coupling calculations in table 3. We see that all three sets of results are in good agreement with each other (5%), at least at energies above 30 eV. The (*R*-matrix) basis I and II results differ by no more than 1% below 30 eV but by 50 eV the target G-states give rise to a 10% increase in the total cross section.

The time-independent and time-dependent results for the electron-impact ionization of Mg^+ are compared with experiment in figure 1. We see that all of the theoretical results clearly favour the measurements of Peart *et al* (1991) over those of Crandall *et al*

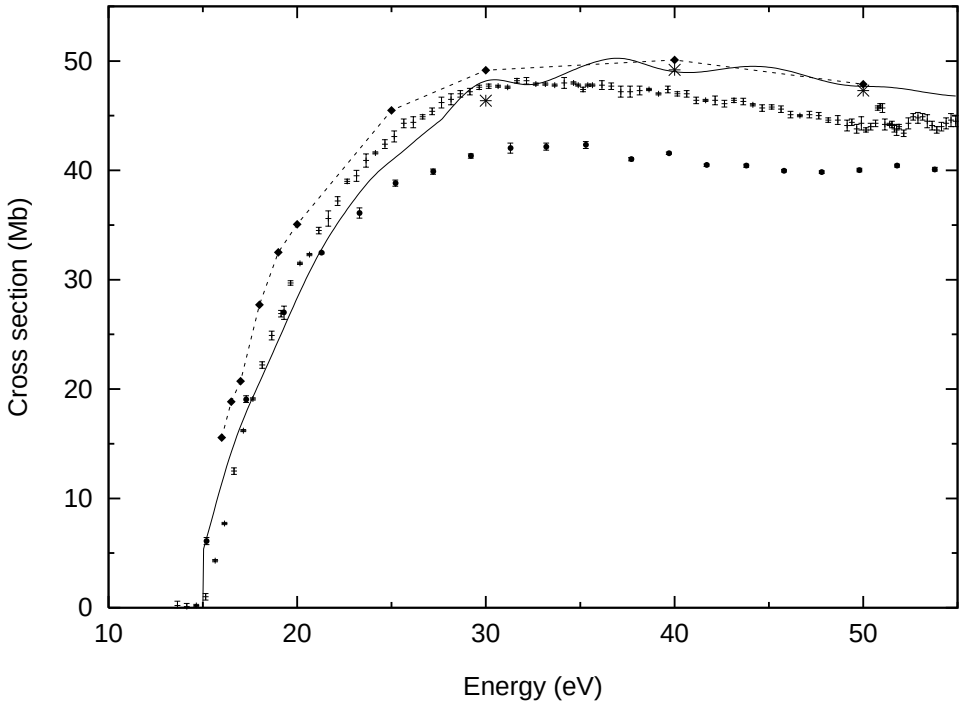

Figure 1. Total electron-impact ionization cross sections for Mg^+. ——, pseudo-state *R*-matrix results (this work); - - - -♦, convergent close-coupling results (this work); ∗, hybrid time-dependent results (this work); upper row of data points (+), measurements by Peart *et al* (1991); lower row of data points (●), measurements by Crandall *et al* (1982).

(1982), above 25 eV. However, at 50 eV all of the theoretical results suggest that even the measurements of Peart *et al* (1991) are, perhaps, somewhat of an underestimate (by up to 10%). The *R*-matrix and convergent close-coupling results agree to better than 1% here and a comparison of our *R*-matrix results for the three bases indicates that our pseudo-state expansion in both $\overline{n}$ and $\overline{l}$ has converged to better than 2% here. The biggest discrepancy between the *R*-matrix and convergent close-coupling results occurs where the cross section is falling-off rapidly, i.e. below 30 eV. Although most sensitive to projection here, its effect was to move the *R*-matrix curve ≈ 1 eV to the left in the figure.

3.2. Al^{2+}

Partial ionization cross sections for Al^{2+} at 45 eV are presented in table 4, where we compare the close-coupling results with themselves and with the distorted-wave results. A key point to note here is that the ^{1}F partial cross section is large and contributes 20% of the total ionization cross section. The comparison is complicated by the oscillatory nature of the *R*-matrix partial cross sections, which vary by ±15%, typically. A least-squares fit over 30–60 eV was carried out to determine the values presented. All three sets of close-coupling results agree to within 15% for $L > 4$. As with Mg^+, it is for the lower-*L* triplets (^{3}P, ^{3}D, ^{3}F, ^{3}G) that the time-dependent and the *R*-matrix results disagree substantially while the agreement between the corresponding singlets is much better. The time-dependent and *R*-matrix results agree to within $\approx 10\%$ for ^{1,3}S, ^{1}D, ^{1}F, ^{1}G and ^{1}H while the convergent

Table 4. Partial ionization cross sections (10^{-18} cm^2) at an incident energy of 45 eV for Al^{2+}.

^{2S+1}L	Distorted-wave (non-exchange)	Time-dependent close-coupling	R-matrix close-coupling	Convergent close-coupling
^{1}0	0.093	0.082	0.080	0.111
^{3}0	0.280	0.007	0.007	0.012
^{1}1	0.318	0.271	0.358	0.479
^{3}1	0.954	0.119	0.172	0.225
^{1}2	0.597	0.603	0.665	0.823
^{3}2	1.790	0.479	0.632	0.829
^{1}3	0.745	1.865	1.870	2.176
^{3}3	2.234	0.237	0.382	0.468
^{1}4	0.375	1.107	1.040	1.199
^{3}4	1.126	0.266	0.371	0.445
^{1}5	0.236	0.828	0.722	0.875
^{3}5	0.707	0.379	0.426	0.485
^{1}6	0.355	1.039	0.909	1.064
^{3}6	1.064	0.258	0.263	0.298
^{1}7	0.262		0.548	0.610
^{3}7	0.785		0.375	0.485
^{1}8	0.155		0.247	0.281
^{3}8	0.466		0.324	0.375
^{1}9	0.081		0.105	0.118
^{3}9	0.242		0.193	0.215
^{1}10	0.038		0.034	0.036
^{3}10	0.114		0.083	0.090

close-coupling results are up to 30% larger than the R-matrix results. The oscillations in the R-matrix results are similar for both the singlet and triplet spin systems and so would not appear to be the cause of the agreement (disagreement) with the time-dependent results for the singlets (triplets). However, there is no clear pattern of agreement or disagreement with the convergent close-coupling results, apart from the improved agreement with increasing L. The time-dependent partial cross sections are invariably smaller than the time-independent ones while the singlet–triplet sum of the distorted-wave $L = 7$ cross sections is somewhat larger than the close-coupling results (by 10–15%). This has implications for the hybrid time-dependent plus distorted-wave total ionization cross sections, which we compare with the time-independent close-coupling results in table 5. The small 'underestimate' of the time-dependent results together with the small 'overestimate' of the distorted-wave results, compared with time-independent close coupling, gives rise to a hybrid total cross section in rather better agreement with the R-matrix results than is perhaps justified by the partial cross sections—recall (table 4) that the results for the ^{1}F partial cross section only differed by 2%. Above 50 eV, the convergent close-coupling and R-matrix results agree to within 10%—the ^{1}F partial cross section contributes 15% of the total at 60 eV and 10% at 80 eV.

The time-independent and time-dependent results for the electron-impact ionization of Al^{2+} are compared with experiment in figure 2. Clearly, the theoretical results show that the measurements by Crandall *et al* (1982) severely underestimate the cross section above 50 eV. Again, at lower energies the R-matrix and convergent close-coupling results show their largest disagreement—by a factor of 1.26 at 35 eV, but the time-dependent hybrid results are still in closer agreement with the R-matrix results there. We see that the small oscillations present in the R-matrix partial cross sections are less apparent in the total cross section. At 45 eV, projection only increased the R-matrix result by 2% but this increases

Table 5. Total ionization cross sections (10^{-18} cm^2) for Al^{2+}.

Energy (eV)	Time-dependent + distorted-wave	*R*-matrix close-coupling	Convergent close-coupling
35	4.78	5.58	7.03
45	9.79	9.96	11.75
60	12.81	12.87	13.47
80	13.32	13.08	13.62

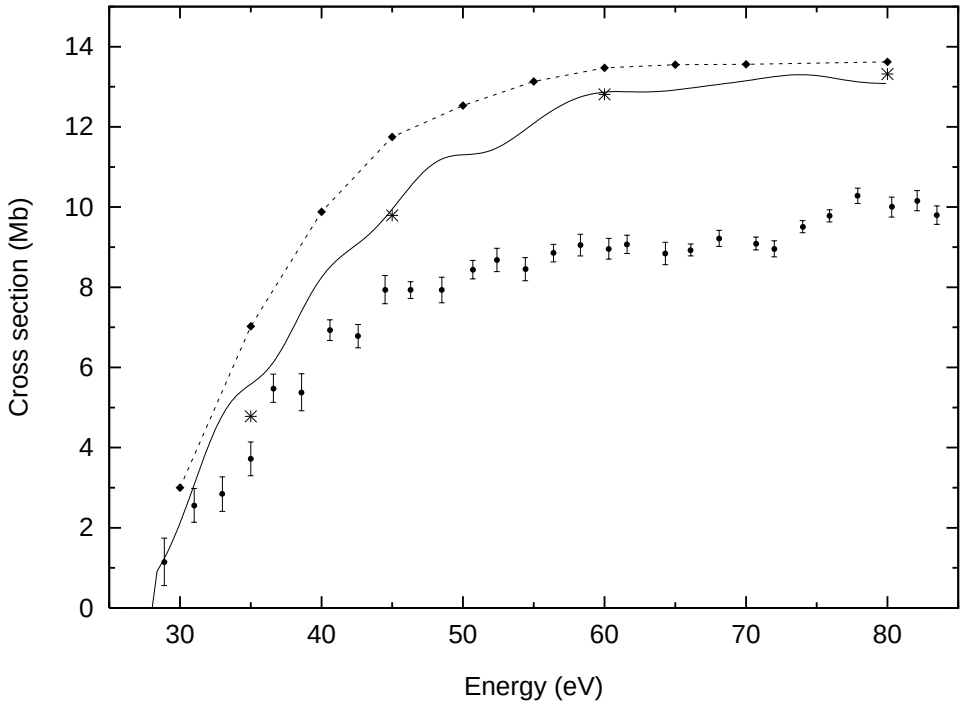

Figure 2. Total electron-impact ionization cross sections for Al^{2+}. ——, pseudo-state *R*-matrix results (this work); - - - -♦, convergent close-coupling results (this work); ∗, hybrid time-dependent results (this work); ●, measurements by Crandall *et al* (1982).

somewhat at lower energies, for example, at 35 eV the cross section was increased by 25%. The *R*-matrix total ionization cross section obtained using basis III is only 4% lower than that obtained from bases I and II at 45 eV.

3.3. Si^{3+}

Given the disagreement noted for Al^{2+}, we have carried out calculations for Si^{3+} as well even though the experimental results of Crandell *et al* (1982) for this ion are subject to large uncertainties. The time-independent and time-dependent cross sections for the total electron-impact ionization of Si^{3+} are presented in table 6 and are compared with experiment in figure 3. The time-dependent hybrid result at 70 eV lies only slightly below the *R*-matrix result (by less than 3%) but the convergent close-coupling result lies 19% higher. We see that the discrepancy between the *R*-matrix and convergent close-coupling results again

Table 6. Total ionization cross sections (10^{-18} cm^2) for Si^{3+}.

Energy (eV)	Time-dependent + distorted-wave	*R*-matrix close-coupling	Convergent close-coupling
60	—	2.83	3.52
70	3.77	3.88	4.60
80	4.57	4.50	4.95
90	5.01	4.88	5.13

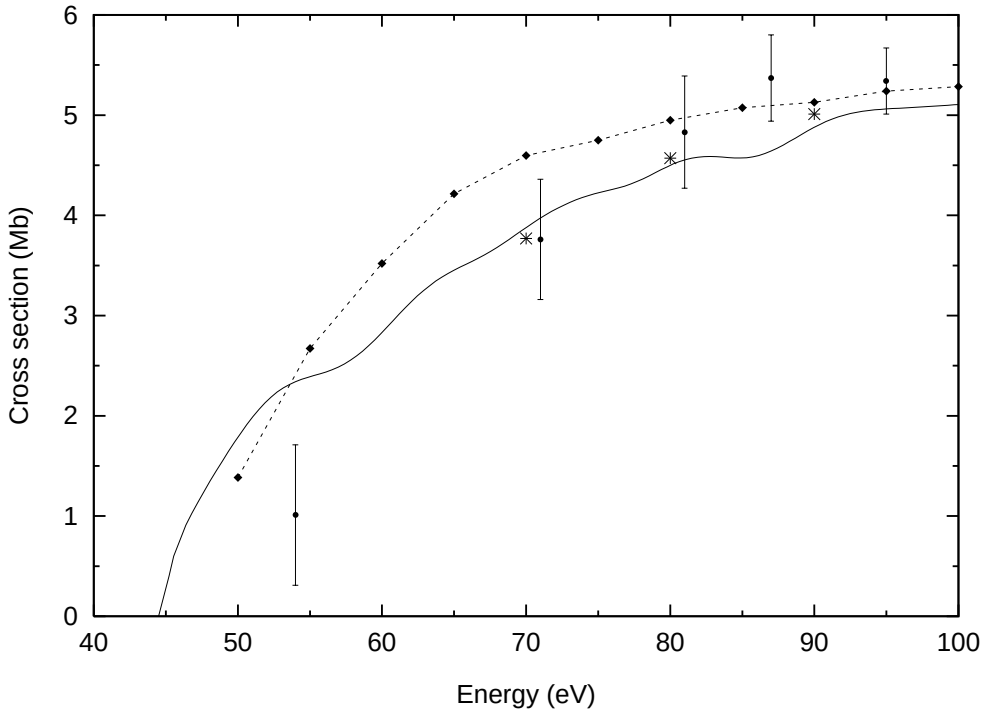

Figure 3. Total electron-impact ionization cross sections for Si^{3+}. ——, pseudo-state *R*-matrix results (this work); - - - -♦, convergent close-coupling results (this work); ∗, hybrid time-dependent results (this work); ●, measurements by Crandall *et al* (1982).

persists over a wide energy range, though all three sets of results converge towards each other at the highest energies considered. The experimental results of Crandell *et al* (1982) do not discriminate between the various theoretical results. As to the partial cross sections (see table 7), they follow the trend established for Mg^+ and Al^{2+}. The time-dependent and *R*-matrix results are in close agreement (to within 10%), except for the $L = 0$–4 triplets, while the convergent close-coupling results are 20–30% larger than the *R*-matrix results.

To try to shed light on the differences between the convergent close-coupling and *R*-matrix results, we have carried out calculations for Si^{3+} and Al^{2+} using the exact same pseudo-state basis. Furthermore, the two sets of Hartree–Fock frozen core orbitals that we used were almost identical, based on their one-electron binding energies. The main (unquantifiable) difference between the *R*-matrix and convergent close-coupling calculations at this stage is the approximation of the Ne-like core by a Hartree–Fock frozen-core potential

Table 7. Partial ionization cross sections (10^{-18} cm^2) at an incident energy of 70 eV for Si^{3+}.

^{2S+1}L	Distorted-wave (non-exchange)	Time-dependent close-coupling	R-matrix close-coupling	Convergent close-coupling
^{1}0	0.042	0.041	0.047	0.055
^{3}0	0.124	0.023	0.004	0.004
^{1}1	0.104	0.166	0.146	0.173
^{3}1	0.313	0.046	0.086	0.109
^{1}2	0.182	0.268	0.217	0.248
^{3}2	0.547	0.201	0.337	0.336
^{1}3	0.251	0.616	0.584	0.809
^{3}3	0.753	0.077	0.153	0.199
^{1}4	0.132	0.325	0.348	0.469
^{3}4	0.395	0.083	0.130	0.153
^{1}5	0.100	0.279	0.277	0.369
^{3}5	0.299	0.081	0.104	0.127
^{1}6	0.163	0.460	0.436	0.586
^{3}6	0.490	0.051	0.058	0.062

in the latter method. However, when we included only 10 s-pseudo-states ($\overline{n} = 3$–12) in our calculations the two sets of partial cross sections differed only by a few per cent, away from any pseudo-resonances. Only by adding higher angular momentum pseudo-states (e.g. basis I) do our two sets of results start to differ more significantly. The calculations at this stage are becoming rather time consuming and it has not been possible to determine why the convergent close-coupling results should lie somewhat, but significantly, above the other two sets of results.

4. Conclusion

In this paper, we have reported on calculations of electron-impact ionization cross sections for Mg^+, Al^{2+} and Si^{3+} that were obtained using both time-independent and time-dependent close-coupling methods. The fact that the time-dependent wavepacket method yields a peak ionization cross section for Mg^+ and Al^{2+} that is in good agreement with those of the two time-independent close-coupling calculations is compelling evidence that the experimental measurements need to be re-examined for these ions, particularly so for the case of Al^{2+}. Even the 10% difference between theory and experiment for Mg^+ is outside of the estimated accuracy of the theoretical cross sections and the experimental uncertainties for this ion. Below the peak cross section, a puzzling discrepancy remains between the convergent close-coupling results and the R-matrix and time-dependent hybrid results, both for Al^{2+} and Si^{3+}. This is surprising given the agreement for Mg^+ and, indeed, the agreement between experiment (Johnston and Burrow 1995) and convergent close-coupling theory for neutral sodium, both for excitation (Bray 1994a) and ionization (Bray 1994b). The results of all three methods are in good agreement for the ionization of Be^+ as well (see Pindzola *et al* 1997). We plan to pursue calculations and comparisons with experiment for the electron-impact ionization of multiply charged Li-like ions in conjunction with new measurements to be undertaken at Oak Ridge National Laboratory (Bannister 1997) to see if we can identify the source of this discrepancy.

Acknowledgments

In this work, NRB was supported by an EPSRC grant (GR/K/14346) with the University of Strathclyde, MSP was supported by a US DoE grant (DE-FG05-96-ER54348) with Auburn University, IB was supported by the Australian Research Council, and DCG was supported by a US DoE grant (DE-FG02-96-ER54367) with Rollins College. The time-dependent calculations were carried out on the Cray T3E-600 at the National Energy Research Supercomputer Center in Berkeley, California, and on the Intel Paragon machines at the Center for Computational Sciences in Oak Ridge, Tennessee.

References

Badnell N R 1986 *J. Phys. B: At. Mol. Phys.* **19** 3827–35
Badnell N R and Gorczyca T W 1997 *J. Phys. B: At. Mol. Opt. Phys.* **30** 2011–19
Bannister M E 1997 Private communication
Bartschat K and Bray I 1996a *J. Phys. B: At. Mol. Opt. Phys.* **29** L577–83
——1996b *Phys. Rev.* A **54** R1002–5
——1997a *J. Phys. B: At. Mol. Opt. Phys.* **30** L109–14
——1997b *Phys. Rev.* A **55** 3236–8
Bartschat K, Hudson E T, Scott M P, Burke P G and Burke V M 1996 *J. Phys. B: At. Mol. Opt. Phys.* **29** 115–23
Berrington K A, Burke P G, Butler K, Seaton M J, Storey P J, Taylor K T and Yu Yan 1987 *J. Phys. B: At. Mol. Opt. Phys.* **20** 6379–97
Berrington K A, Eissner W B and Norrington P H 1995 *Comput. Phys. Commun.* **92** 290–420
Bray I 1994a *Phys. Rev.* A **49** 1066–82
——1994b *Phys. Rev. Lett.* **73** 1088–90
——1995 *J. Phys. B: At. Mol. Opt. Phys.* **28** L247–54
——1997 *Phys. Rev. Lett.* **78** 4721–4
Bray I and Clare B 1997 *Phys. Rev.* A **56** R1694–6
Bray I and Fursa D V 1995 *Phys. Rev.* A **52** 1279–97
——1996 *Phys. Rev.* A **54** 2991–3004
Bray I and Stelbovics A T 1993 *Phys. Rev. Lett.* **70** 746–9
——1995 *Comput. Phys. Commun.* **85** 1–17
Burgess A 1974 *J. Phys. B: At. Mol. Phys.* **7** L364–7
Burgess A, Hummer D G and Tully J A 1970 *Phil. Trans. R. Soc.* **266** 225–79
Burke P G and Berrington K A 1993 *Atomic and Molecular Processes—An R-matrix Approach* (Bristol: IOP)
Christiansen P A, Lee Y S and Pitzer K S 1979 *J. Chem. Phys.* **71** 4445–50
Crandall D H, Phaneuf R A, Falk R A, Belić D S and Dunn G H 1982 *Phys. Rev.* A **25** 143–53
Froese Fischer C 1991 *Comput. Phys. Commun.* **64** 369–98
Gallaher D F 1974 *J. Phys. B: At. Mol. Phys.* **7** 362–70
Gorczyca T W and Badnell N R 1997 *J. Phys. B: At. Mol. Opt. Phys.* **30** 3897–911
Gorczyca T W, Pindzola M S, Badnell N R and Griffin D C 1994 *Phys. Rev.* A **49** 4682–92
Hudson E T, Bartschat K, Scott M P, Burke P G and Burke V M 1996 *J. Phys. B: At. Mol. Opt. Phys.* **29** 5513–26
Hummer D G, Berrington K A, Eissner W, Pradhan A K, Saraph H E and Tully J A 1993 *Astron. Astrophys.* **279** 298–309
Johnston A R and Burrow P D 1995 *Phys. Rev.* A **51** R1735–7
Kato D and Watanabe S 1995 *Phys. Rev. Lett.* **74** 2443–6
Marchalant P J, Bartschat K and Bray I 1997 *J. Phys. B: At. Mol. Opt. Phys.* **30** L435–40
Peart B, Thomason J W G and Dolder K 1991 *J. Phys. B: At. Mol. Opt. Phys.* **24** 4453–61
Pindzola M S and Robicheaux F 1996 *Phys. Rev.* A **54** 2142–5
——1997 *Phys. Rev.* A **55** 4617–20
Pindzola M S, Robicheaux F, Badnell N R, and Gorczyca T W 1997 *Phys. Rev.* A **56** 1994–9
Pindzola M S and Schultz D R 1996 *Phys. Rev.* A **53** 1525–36
Yamani H A and Reinhardt W P 1975 *Phys. Rev.* A **11** 1144–56
Younger S M 1980 *Phys. Rev.* A **22** 111–17
——1981 *Phys. Rev.* A **24** 1272–7